

Creating Physiologically Realistic Vertebral Fractures in a Cervine Model

Nicole C. Corbiere

Department of Mechanical and Aeronautical Engineering,
Clarkson University,
Potsdam, NY 13699

Kathleen A. Lewicki

Department of Mechanical and Aeronautical Engineering,
Clarkson University,
Potsdam, NY 13699;
Thayer School of Engineering,
Dartmouth College,
Hanover, NH 03755

Kathleen A. Issen

Department of Mechanical and Aeronautical Engineering,
Clarkson University,
Potsdam, NY 13699

Laurel Kuxhaus¹

Department of Mechanical and Aeronautical Engineering,
Clarkson University,
Potsdam, NY 13699
e-mail: lkuxhaus@clarkson.edu

Approximately 50% of women and 25% of men will have an osteoporosis-related fracture after the age of 50, yet the micromechanical origin of these fractures remains unclear. Preventing these fractures requires an understanding of compression fracture formation in vertebral cancellous bone. The immediate research goal was to create clinically relevant (midvertebral body and endplate) fractures in three-vertebrae motion segments subject to physiologically realistic compressional loading conditions. Six three-vertebrae motion segments (five cervine, one cadaver) were potted to ensure physiologic alignment with the compressive load. A 3D microcomputed tomography (microCT) image of each motion segment was generated. The motion segments were then preconditioned and monotonically compressed until failure, as identified by a notable load drop (48–66% of peak load in this study). A second microCT image was then generated. These three-dimensional images of the cancellous bone structure were inspected after loading to qualitatively identify fracture location and type. The microCT images show that the trabeculae in the cervine specimens are oriented similarly to those in the cadaver specimen. In the cervine specimens, the peak load prior to failure is highest for the L4–L6 motion segment, and decreases for each cranially adjacent motion segment. Three motion segments formed endplate fractures and three formed midvertebral body fractures; these two fracture types correspond to clinically observed fracture modes. Examination of normalized-load versus normalized-displacement curves suggests that the size (e.g., cross-sectional area) of a vertebra is not the only factor in the mechanical response in healthy vertebral specimens. Furthermore, these normalized-load versus normalized-displacement data appear to be grouped by the fracture type. Taken together, these results show that (1) the loading protocol creates fractures that appear physiologically realistic in vertebrae, (2) cervine vertebrae

fracture similarly to the cadaver specimen under these loading conditions, and (3) that the prefracture load response may predict the impending fracture mode under the loading conditions used in this study. [DOI: 10.1115/1.4027059]

Keywords: motion segments, microcomputed tomography, compression, animal model, spine, endplate fracture, vertebral body fracture

Introduction

Vertebral compression fractures are a common sequela of osteoporosis and also occur with trauma in an otherwise healthy patient. In both cases, the vertebrae are unable to withstand the compressive load applied and the failure occurs in both the cortical and cancellous bone. Without accurate predictive measures of in whom and where these fractures will occur, there is little hope for reducing patient morbidity. Approximately, 50% of women and 25% of men will have an osteoporosis-related fracture after the age of fifty [1]. With 750,000 people suffering from osteoporotic vertebral fractures annually [2] and an estimated underdiagnosis of 45% in North America [3], a priori clinical prediction of vertebral fracture could identify vertebrae at the highest risk of fracture and make preventative intervention possible. Toward this long-term goal, this work studies fractures created in vertebrae.

To conduct a clinically relevant characterization of vertebral fractures at the micro-architectural level, the fractures must be created under physiologic loading conditions. Historically, cores of cancellous bone [4–7] or vertebral bodies with the endplates removed [8] were used to determine mechanical response; however, this does not necessarily replicate in vivo loading or boundary conditions. Similarly, others have compressed individual vertebrae with intact endplates but no surrounding intervertebral disks [9,10], applying the compressive load directly to the endplates instead of via the center of the intervertebral disk as would occur physiologically [11–13]. Two-vertebra motion segments [14,15] have been used to quantify differences in mechanical response, such as the relationship between tissue maturation and the compressive/tensile stiffnesses in vertebrae. While these works have provided useful insights into vertebral mechanical response and failure (e.g., cancellous bone governs vertebral damage behavior), these specimen configurations do not replicate in vivo loading or boundary conditions as they do not include an intervertebral disc on either side of the vertebra under investigation. To achieve this, a minimum of a three-vertebra motion segment is necessary [16,17], in which load is transferred via the intervertebral disks to the middle vertebra.

For this study, cervine thoracic and lumbar vertebrae are used as a model. Though not widely used, cervine vertebrae are primarily loaded in axial compression [18]. Additionally, the lower thoracic (T10–T13) and upper lumbar (L1–L4) regions of cervine spines have bone mineral densities (BMDs) with T-scores of -0.7 and 0 , respectively, indicating nearly comparable BMDs to those of human vertebrae in the same regions [19]. Thus, cervine vertebrae were chosen for this developmental work.

The purpose of the present work was to develop a method to apply physiologically realistic loading conditions to vertebrae and create clinically relevant vertebral fractures. Fractures created in cervine vertebrae were compared to those created in a cadaveric vertebral motion segment. This work identifies and describes fractures via microcomputed tomography (μ CT) imaging. This is noteworthy as micro-architectural inspection of fractures created using three-vertebra motion segments has not been previously reported.

Methods

Five three-vertebra motion segments were dissected from a fresh-frozen male cervine spine of approximately 18 months of age (Nolt's Custom Meat Cutting, Lowville, NY). Each motion segment included intact intervertebral disks cranial and caudal to

¹Corresponding author.

Manuscript received October 4, 2013; final manuscript received February 6, 2014; accepted manuscript posted March 6, 2014; published online May 6, 2014. Assoc. Editor: Kristen Billiar.

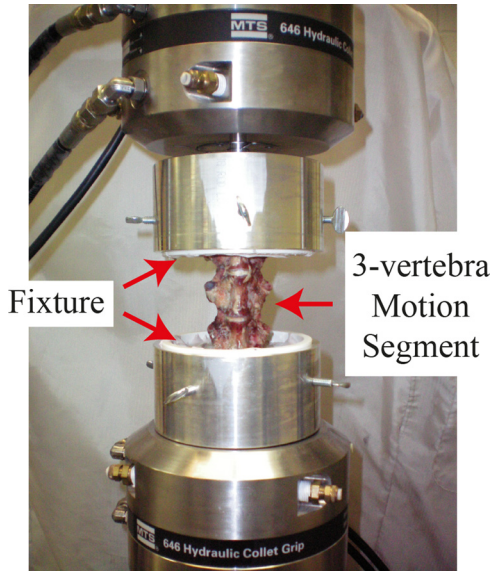


Fig. 1 Load frame fixture with potted specimen

the middle vertebra. The five motion segments were: T2-T4, T8-T10, T11-T13, L1-L3, and L4-L6. One cadaver motion segment, L3-L5, from a 58 yr old female donor (Medcure, Portland, OR) was also prepared.

Alignment of Vertebrae With Loading Direction. Before compressing the six vertebral motion segments, the cranial and caudal (or superior and inferior) vertebrae were embedded in Bondo™ (Auto Body Filler, 3M, St. Paul, MN). A custom potting alignment apparatus was used to (1) align the centers of the intervertebral disks with the direction of the load to be applied during compression and (2) produce the cranial and caudal (or superior and inferior) end caps. The intervertebral disks were centered in the endcaps. Vertical alignment of the motion segment was ensured during this potting process by inserting a metal rod surrounded by a garolite tube (Machinable Garolite (LE), McMaster Carr, Cleveland, OH) into the spinal cord canal. The rod, but not the tube, was removed prior to loading.

Imaging. The motion segments were imaged using a μ CT scanner (GE Phoenix Nanotom, General Electric, Wunstorf Germany) both before and after compression testing. Each specimen was scanned at 80–100 kV and 310–380 μ A, that produced a resolution of 21.7–29.6 μ m. VGSTUDIO MAX 2.2 software (Volume Graphics GmbH, Heidelberg, Germany) was used to inspect the post-compression images to locate the fracture.

Loading. The end caps were placed in a custom fixture to interface with the load frame (Instron 1331, load cell model 3116–135, Norwood, MA) such that the compressive load was centered over the center of the intervertebral disks (Fig. 1). Specimens were preconditioned in load control from 100N to 250N for 10 cycles [9,10]. Specimens were then compressed using displacement control at a rate of 0.5 mm/min [10] and load was monitored via a real-time load–displacement curve. TESTWARESX software (MTS Systems Corporation, Eden Prairie, MN) was used to control the load frame for this quasi-static test procedure. The test was stopped after the first notable load drop, which should correspond to fracture formation. Terminating the test at this point prevented extensive damage that could destroy evidence of the initial fracture region. After compression, specimens were rescanned using the procedure described above.

Analysis Procedure. The reconstructed volume from the μ CT scans was visually inspected to identify the fracture region. This

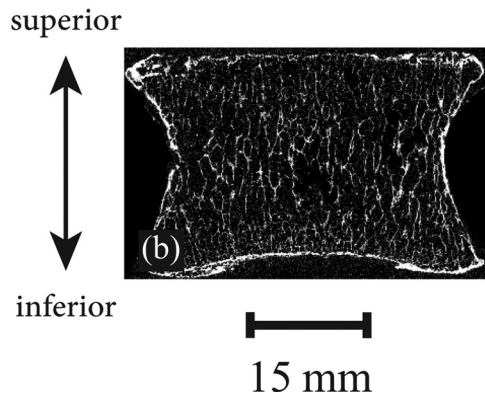
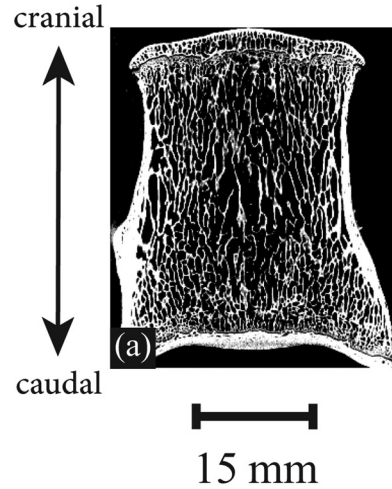


Fig. 2 MicroCT image of cross-section from (a) cervine L4 lumbar vertebra and (b) cadaver L4 lumbar vertebra

inspection permitted a qualitative description of each fracture and its location. There were notable differences in vertebral body dimensions for the six motion segments. For monolithic materials, specimen geometry effects are removed by analyzing stress versus strain. These measures are not strictly applicable to a motion segment; instead, a normalization method was used to approximate the removal of geometry effects. The load and displacement for each specimen were normalized by a selected crosshead displacement and the corresponding load at that displacement. For this study, the selected normalization displacement was 5.0 mm, the highest displacement prior to the notable load drop for any specimen.

Results

Figure 2 shows μ CT images of the cross-sections of intact cervine and cadaver lumbar vertebrae. Note that the trabeculae in both vertebrae are predominately parallel to the long-axis of the spine. The orientation of these trabeculae confirms that the dominant *in vivo* loading is axial compression, in both quadrupeds and human bipeds, as reported by Smit [18].

Fractures were created in five three-vertebra motion segments from one cervine spine and one motion segment from a cadaver spine. Similar mechanical responses were observed in the cervine and cadaver specimens. No disc herniation was observed. The load–displacement curves for all specimens (Fig. 3) are nonmonotonic; that is, periodic load spikes occur. These are likely caused by facet locking or other physical interference. During initial loading, the curves exhibit a roughly linear trend up to approximately half of the peak load. Subsequently, in most specimens, the slope decreases leading up to the peak load. The most notable feature of each curve is a large load drop, likely corresponding to fracture formation.

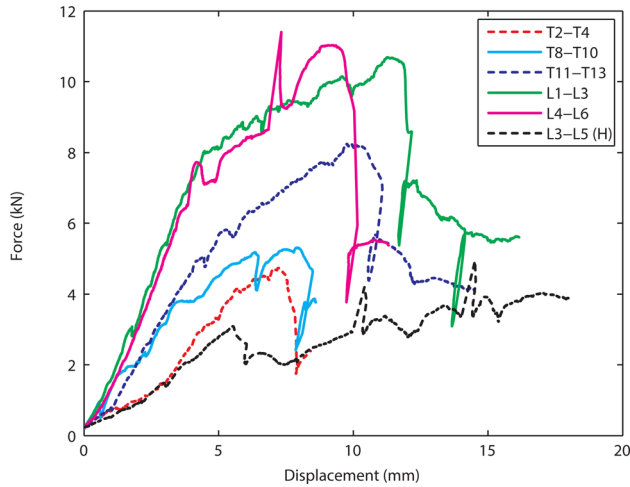


Fig. 3 Load–displacement curves for all three-vertebra motion segments. Dashed lines indicate endplate fractures and solid lines indicate midvertebral body fractures. The cadaver specimen curve is marked (H).

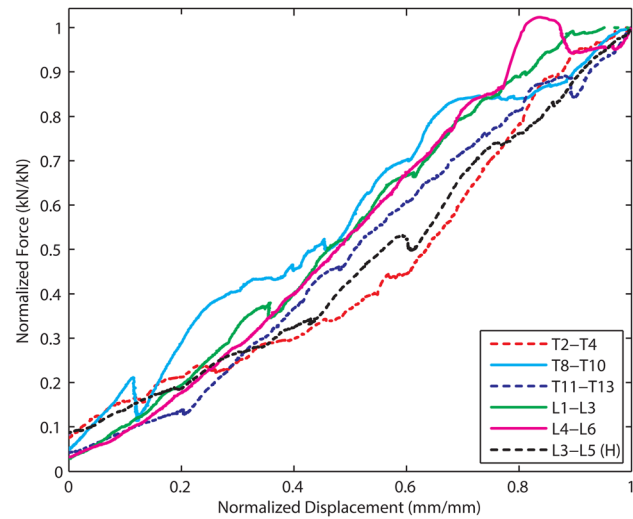


Fig. 5 Normalized-load versus normalized-displacement curves for all vertebral motion segments. Dashed lines indicate endplate fractures and solid lines indicate midvertebral body fractures. The cadaver specimen curve is marked (H).

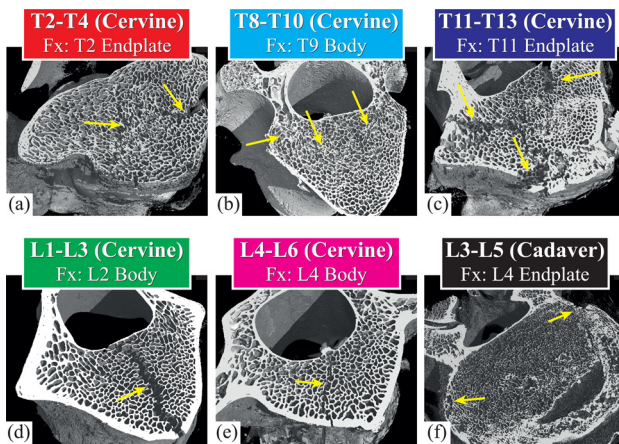


Fig. 4 Fracture type and location (indicated by arrows) for each motion segment. (Supplemental material for 3D fly-through videos of each cervine specimen is available under the “Supplemental Data” tab for this paper on the ASME Digital Collection)

As shown in Fig. 4, the T2-T4 segment fractured in the caudal endplate region of the T2 vertebra. The T8-T10 segment formed a conical fracture in the cranial end of the T9 vertebral body, resembling a cup-and-cone fracture in ductile metals. The T11-T13 segment fractured in the T11 caudal endplate. The L1-L3 and L4-L6 segments each fractured in the middle vertebral body of the segment. The L1-L3 fracture resembles a wine glass with part of the cup missing on the posterior side [20]. In L4-L6, there is a vertical fracture in the upper portion of the L5 vertebral body and a horizontal fracture (roughly along the frontal plane) in the lower portion of the L5 vertebral body; the upper portion of the vertebra is offset laterally to the right along the horizontal fracture. The cadaver motion segment (L3-L5) fractured in the cranial endplate of the L4 vertebra. MicroCT images of the fractures are shown in Fig. 4 and fly-through animations of the specimens are available on the “Supplemental Data” tab for this paper on the ASME Digital Collection.

Discussion

For the cervine specimens, the peak load value is highest for the L4-L6 motion segment (Fig. 3), with peak loads systematically decreasing for each cranially adjacent motion segment. This result could be attributed to the relative increase in cross-sectional area [19] of the caudal vertebral bodies compared to those cranially.

The load drops for the cervine specimens are relatively large, ranging from 48–66% of the peak load. For the L3-L5 (cadaver) motion segment, there are several smaller load drops suggesting small fracture events. The cadaver motion segment was loaded to approximately 4.9 kN, a load that has previously fractured vertebrae without a large load drop [9].

Note that the first 4.0 mm of the load–displacement curves for the L3-L5 cadaver motion segment and the T2-T4 cervine motion segment are nearly coincident (Fig. 3). This result is similar to that of Haddock et al. who reported strikingly similar material stiffnesses for bovine and cadaver cancellous bone cores before failure occurred [21]. After a displacement of 4.0 mm, the load for the cervine T2-T4 specimen continues to increase up to approximately 7.0 mm, while the load for the cadaver L3-L5 motion segment has a local peak at around 5.0 mm. The differences in mechanical response after the initial loading are likely due to differences in specimen geometries and micro-architecture, which will influence fracture initiation and propagation.

Two distinct fracture types emerged from this work: 1) an endplate fracture in the cranial portion of the motion segment (Figs. 4(a), 4(c), and 4(f)), and 2) a midvertebral fracture in the middle vertebra of the motion segment (Figs. 4(b), 4(d), and 4(e)). The endplate fractures observed here are similar to those that occur with trauma in healthy humans (such as ejection from military aircrafts [22] or body blast loading scenarios experienced by pilots [23]), or in those with osteogenesis imperfecta [24], despite the fact that the fractures in the current work were created under slower loading conditions than typically seen in vivo. The cadaver specimen experienced a traumatic endplate fracture; this result is perhaps expected, since the cadaver donor was 58 yr of age with no indications of osteoporosis or osteopenia per the provided data sheet. The midvertebral body fractures in the three cervine segments are similar in appearance to osteoporotic vertebral fractures that occur in humans [25] (note that the anterior–posterior fracture is atypical, Figs. 4(d) and 4(e)). This is intriguing in that the cervine population is assumed to be healthy (i.e., nonosteoporotic). While the cervine specimens did not have osteoporosis, they were from a skeletally immature donor (a juvenile deer of approximately 18 months of age), in the midst of pubertal development [26]. The skeletal structure, including the cancellous bone, was still in development; the bone tissue was not fully mineralized, resulting in reduced tissue stiffness. Thus, trabeculae could be susceptible to local bending and buckling, predisposing some specimens to midvertebral body fractures. Future work is needed to investigate the effects of cervine age on the vertebral mechanical response.

Figure 5 shows that the normalized-load versus normalized-displacement curves for the motion segments are generally similar, although not exactly coincident. This implies that the overall failure process is similar for each motion segment (i.e., all motion segments are forming some type of fracture). The dissimilarities in the normalized curves of Fig. 5 suggest that differences in motion segment geometry, and perhaps cancellous bone micro-architecture (e.g., geometry and organization of trabeculae) influence the failure process, resulting in different fracture types (endplate versus midvertebral body) and variations within type.

For illustration purposes, in Fig. 5, the curves for specimens with endplate fractures (T2-T4, T11-T13, and L3-L5) are dashed, while the curves for specimens with midvertebral body fractures (T8-T10, L1-L3, and L4-L6) are solid. Between 0.3 and 0.8 mm/mm the three curves for endplate fractures fall below the three curves for midvertebral body fractures. This sample size is not sufficient to conclude that this difference in mechanical response is characteristic of fracture type; however, it is an interesting result that will be investigated in future work.

This study has several limitations. The first is use of cervine vertebrae as a proxy for cadaver vertebrae. The cervine vertebral bodies are notably different in aspect ratio from human vertebrae, yet their trabecular structures are similarly aligned (Fig. 1), and other researchers have suggested that cervine vertebrae are suitable proxies for cadaver vertebrae [19,27]. Furthermore, cervine vertebrae are locally available in many regions, typically discarded during the butchering process. Conversely, the vertebrae of other species (e.g., porcine) are included in popular cuts of meat. Future tests can confirm that additional cervine specimens behave similarly to the motion segments used here, which all came from a single cervine donor. This study used a straight spinal cord canal in the potting process. While a healthy human spine has a characteristic curvature, this angle of curvature between adjacent vertebrae is small and the dominant loading is still parallel to the spinal canal, transferred from the intervertebral disks to the vertebrae [18]; therefore, use of an initially straight spinal cord canal is acceptable. Finally, lateral muscle forces applied to the spine in vivo were not replicated in our test procedure. In this study, axial compressive loads were applied; this is the direction of dominant loading as evidenced by the trabecular orientation. Therefore, lateral muscle forces are likely smaller in comparison and could be included in future work.

This work is significant for several reasons. It is the first to combine three-dimensional imaging of cervine vertebrae with mechanical compressional loading. The potting and compression processes apply physiologically realistic loading conditions to the motion segment, resulting in clinically relevant vertebral fractures: endplate fractures and midvertebral body fractures. From μ CT images, trabeculae in both cervine and cadaver vertebrae are preferentially aligned with the axial direction, corresponding to the in vivo maximum compression loading direction for both deer and humans. Similar mechanical responses (e.g., normalized-load versus normalized-displacement curves prior to fracture) and similar fracture types were observed in both cervine and cadaver specimens. These results taken together suggest that cervine vertebrae have the potential to be proxies for cadaver vertebrae under axial compression conditions, and that the methods presented here can be used in future biomechanical studies of vertebral fracture under physiologically realistic loading conditions. Finally, preliminary results suggest a possible relationship between the prefracture loading response and the resulting fracture type (endplate versus midvertebral body); additional work will focus on understanding this relationship.

Future work may include different loading regimes, such as cyclic loading, to simulate activities of daily living, and a detailed comparison of the fracture patterns to those formed in humans. In conclusion, vertebral fractures have been created in cervine motion segments, that responded similarly to the cadaver vertebral motion segment subjected to similar loading conditions. The fractures are of the type expected in analogous clinical scenarios, and

thus this method for creating physiologically realistic fractures is deemed appropriate for future use.

Acknowledgment

The authors thank undergraduate researcher Cassandra Christman for her help with the experiments and Dr. Mario Ciani for his assistance with the cadaver specimen preparation. Additional graduate student support was provided by an NSF S-STEM Award (DUE – 1060382).

References

- [1] NOF, 2013, "National Osteoporosis Foundation—Debunking the Myths, Fast Facts—Fractures." Available at: <http://www.Nof.Org>, 2011.
- [2] AANS, 2007, "American Association of Neurological Surgeons—Vertebral Compression Fractures." Available at: <http://www.Aans.Org>, 2013.
- [3] Delmas, P. D., van de Langerijt, L., and Watts, N. B., 2005, "Underdiagnosis of Vertebral Fractures is a Worldwide Problem: The IMPACT Study," *J. Bone Miner. Res.*, **20**(4), pp. 557–563.
- [4] Rapillard, L., Charlebois, M., and Zysset, P. K., 2006, "Compressive Fatigue Behavior of Human Vertebral Trabecular Bone," *J. Biomech.*, **39**(11), pp. 2133–2139.
- [5] Keller, T. S., 1994, "Predicting the Compressive Mechanical Behavior of Bone," *J. Biomech.*, **27**(9), pp. 1159–1168.
- [6] Race, A., Miller, M. A., and Mann, K. A., 2010, "Novel Methods to Study Functional Loading Micromechanics at the Stem–Cement and Cement–Bone Interface in Cemented Femoral Hip Replacements," *J. Biomech.*, **43**(4), pp. 788–791.
- [7] Race, A., Mann, K. A., and Edidin, A. A., 2007, "Mechanics of Bone/PMMA Composite Structures: An in vitro Study of Human Vertebrae," *J. Biomech.*, **40**(5), pp. 1002–1010.
- [8] Ebbesen, E. N., Thomsen, J. S., and Beck-Nielsen, H., 1999, "Lumbar Vertebral Body Compressive Strength Evaluated by Dual–Energy X-Ray Absorptiometry, Quantitative Computed Tomography, and Ashing," *Bone*, **25**(6), pp. 713–724.
- [9] Kopperdahl, D. L., Pearlman, J. L., and Keaveny, T. M., 2000, "Biomechanical Consequences of an Isolated Overload on the Human Vertebral Body," *J. Orthop. Res.*, **18**(5) pp. 685–690.
- [10] Buckley, J. M., Kuo, C. C., and Cheng, L. C., 2009, "Relative Strength of Thoracic Vertebrae in Axial Compression Versus Flexion," *Spine J.*, **9**(6), pp. 478–485.
- [11] Brown, S. H. M., Gregory, D. E., and McGill, S. M., 2008, "Vertebral End-Plate Fractures as a Result of High Rate Pressure Loading in the Nucleus of the Young Adult Porcine Spine," *J. Biomech.*, **41**(1), pp. 122–127.
- [12] Tsai, K., Lin, R., and Chang, G., 1998, "Rate-Related Fatigue Injury of Vertebral Disc Under Axial Cyclic Loading in a Porcine Body-Disc-Body Unit," *Clin. Biomech.*, **13**(Suppl 1), pp. S32–S39.
- [13] Moroney, S. P., Schultz, A. B., and Miller, J. A. A., 1988, "Load-Displacement Properties of Lower Cervical Spine Motion Segments," *J. Biomech.*, **21**(9), pp. 769–779.
- [14] Nuckley, D. J., and Ching, R. P., 2006, "Developmental Biomechanics of the Cervical Spine: Tension and Compression," *J. Biomech.*, **39**(16), pp. 3045–3054.
- [15] Rostedt, M., Ekström, L., and Broman, H., 1998, "Axial Stiffness of Human Lumbar Motion Segments, Force Dependence," *J. Biomech.*, **31**(6), pp. 503–509.
- [16] Stokes, I. A. F., 1988, "Mechanical Function of Facet Joints in the Lumbar Spine," *Clin. Biomech.*, **3**(2), pp. 101–105.
- [17] Boisclair, D., Mac-Thiong, J., and Parent, S., 2011, "Effect of Spinal Level and Loading Conditions on the Production of Vertebral Burst Fractures in a Porcine Model," *ASME J. Biomech. Eng.*, **133**, p. 094503.
- [18] Smit, T. H., 2002, "The Use of a Quadruped as an in vivo Model for the Study of the Spine—Biomechanical Considerations," *Eur. Spine J.*, **11**, pp. 137–144.
- [19] Kumar, N., Kukreti, S., and Ishaque, M., 2000, "Anatomy of Deer Spine and Its Comparison to the Human Spine," *Anat. Rec.*, **260**(2), pp. 189–203.
- [20] Corbiere, N. C., Kafka, O. L., and Issen, K. A., 2013, "Cancellous Bone Fracture Visualization Method," American Society of Biomechanics 37th Annual Meeting Conference Proceedings, American Society of Biomechanics, ed., Vol. 37, pp. 453–454.
- [21] Haddock, S. M., Yeh, O. C., and Mummaneni, P. V., 2004, "Similarity in the Fatigue Behavior of Trabecular Bone Across Site and Species," *J. Biomech.*, **37**(2) pp. 181–187.
- [22] Stemper, B. D., Storvik, S. G., and Yoganandan, N., 2011, "A New PMHS Model for Lumbar Spine Injuries During Vertical Acceleration," *ASME J. Biomech. Eng.*, **133**(8), p. 081002.
- [23] Yoganandan, N., Stemper, B. D., and Pintar, F. A., 2013, "Cervical Spine Injury Biomechanics: Applications for Under Body Blast Loadings in Military Environments," *Clin. Biomech.*, **28**(6), pp. 602–609.
- [24] Ben Amor, I. M., Roughley, P., and Glorieux, F. H., 2013, "Skeletal Clinical Characteristics of Osteogenesis Imperfecta Caused by Haploinsufficiency Mutations in COL1A1," *J. Bone Miner. Res.*, **28**(9), pp. 2001–2007.
- [25] Keller, T. S., Harrison, D. E., and Colloca, C. J., 2003, "Prediction of Osteoporotic Spinal Deformity," *Spine*, **28**(5), pp. 455–462.
- [26] Gordon, I., 2004, *Reproductive Technologies in Farm Animals*, CABI Publishing, UK, pp. 339.
- [27] Kumar, N., Kukreti, S., and Ishaque, M., 2002, "Functional Anatomy of the Deer Spine: An Appropriate Biomechanical Model for the Human Spine?" *Anat. Rec.*, **266**(2), pp. 108–117.